P H Y S I C A L   R E V I E W   L E T T E R S

Noncoplanar Magnetic Ordering Driven by Itinerant Electrons on the Pyrochlore Lattice

Gia-Wei Chern

Department of Physics, University of Wisconsin, Madison, Wisconsin 53706, USA

Exchange interaction tends to favor collinear or coplanar magnetic orders in rotationally invariant spin systems. Indeed, such magnetic structures are usually selected by thermal or quantum fluctuations in highly frustrated magnets. Here we show that a complex *noncoplanar* magnetic order with a quadrupled unit cell is stabilized by itinerant electrons on the pyrochlore lattice. Specifically, we consider a Kondo-lattice model with classical localized moments at quarter filling. The electron Fermi "surface" at this filling factor is topologically equivalent to three intersecting Fermi circles. Perfect nesting of the Fermi lines leads to magnetic ordering with multiple wave vectors and a definite handedness. The chiral order might persist without magnetic order in a chiral spin liquid at finite temperatures.

Magnets with geometrical frustration have fascinated physicists for more than a decade as models of strongly interacting systems. A prominent example of magnetic frustration in high dimensions is the nearest-neighbor anti-ferromagnet on the *pyrochlore* lattice shown in Fig. 1(a). For classical Heisenberg spins, strong geometrical frustration prevents the magnet from settling in a long-range magnetic order even at zero temperature [1]. Instead, the ground state retains a finite zero-point entropy and is susceptible to small perturbations such as anisotropies, further-neighbor couplings, and dipolar interactions. In real compounds, magnetic frustration is often relieved when spins couple to other degrees of freedom. An intensively studied case is spin-lattice coupling in chromium spinels where the magnetic transition is accompanied by a lattice distortion [2–4]. Another well known example is magnetic phase transition facilitated by orbital order in frustrated spin-orbital systems [5–8].

Metallic pyrochlore magnets such as Kondo-lattice or double-exchange models pose a different challenge for theorists due to the nonlocal nature of the electron-mediated interactions. Indeed, despite considerable effort [9–12], a complete picture of the phase diagram is still lacking. An early study of the double-exchange model on a pyrochlore lattice revealed a rich mean-field phase diagram [9]. However, the calculation considered only magnetic orders which preserve the lattice translational symmetry, hence precluding magnetic structures with multiple wave vectors. A recent Monte Carlo study of the same model provided an unbiased phase diagram at large Hund's coupling [11]. In particular, a peculiar state with electronic phase separation was observed. Magnetic orders in the weak-coupling regime remain unclear.

Magnetic ordering in frustrated metallic systems depends in an intricate way on the underlying electron Fermi surface. At small filling factors, localized spins interact with each other through a long-range oscillatory Ruderman-Kittel-Kasuya-Yosida (RKKY) interaction mediated by the

electrons. A Monte Carlo simulation of pyrochlore spin-ice with RKKY interaction showed that the sign of the effective Curie-Weiss constant as well as that of nearest-neighbor coupling vary with the electron Fermi wave vector [10]. This in turn determines magnetic ordering at low temperatures: The magnetic state of individual tetrahedra evolves from the 2-in–2-out ferromagnetic state to the all-in or all-out configurations with increasing electron density.
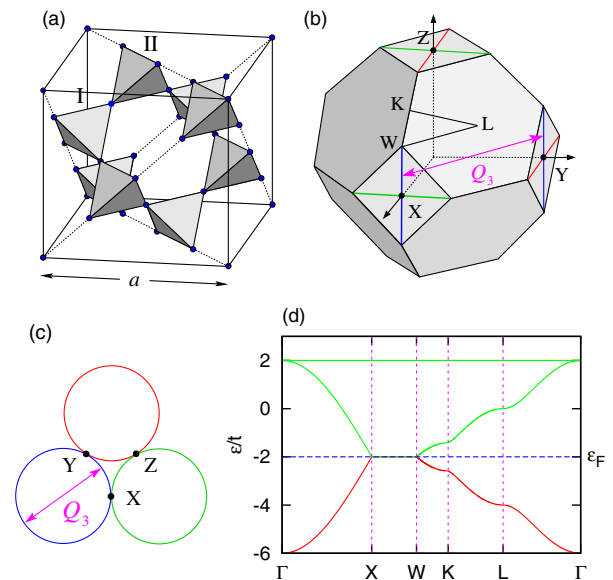

FIG. 1 (color online).   (a) A conventional cubic unit cell of the pyrochlore lattice. I and II denote the two types of tetrahedra with different orientations. The underlying Bravais lattice is a face-centered cubic (fcc) lattice. (b) First Brillouin zone of the fcc lattice. At quarter filling, the electron Fermi surface consists of diagonal lines on the square face of the Brillouin zone. (c) Topologically, these Fermi lines are equivalent to three closed loops intersecting at the X points of the Brillouin zone. (d) Band structure of the tight-binding model on the pyrochlore lattice. The segment XW corresponds to one-quarter of a Fermi circle at quarter filling.

The geometry of the electron Fermi surface also plays an important role in determining the magnetic instability of itinerant systems, particularly at commensurate filling factors. A canonical example is Néel ordering caused by perfect Fermi surface nesting that occurs at a half-filled square-lattice Hubbard model. While the resulting spin structure is collinear in a bipartite square lattice, it was shown that the nesting effect on a triangular lattice leads to a rare noncoplanar magnetic order at filling factors 3/4 and 1/4 [13–15]. This chiral magnetic structure induces a spontaneous quantum Hall effect in the absence of an external magnetic field. Although a long-range magnetic order cannot survive thermal fluctuations in two spatial dimensions, the discrete chiral order persists up to a finite temperature [13].

In this Letter, we demonstrate that the ground state of an isotropic Kondo-lattice model on the pyrochlore lattice is magnetically ordered with a noncoplanar spin structure and a definite chirality. The noncoplanar magnetic order stems from a weak-coupling instability caused by perfect nesting of Fermi "circles" at quarter filling; the quadrupled magnetic unit cell contains 16 spins. In contrast to the triangular-lattice model [13], this noncoplanar spin order does not support a spontaneous Hall insulator because of a trivial Berry phase acquired by the electrons when traversing a tetrahedron. The magnetic structure itself, on the other hand, has a definite handedness and is characterized by a nonzero chiral order parameter.

It should be pointed out that, although chiral magnetic orders have been reported in metallic pyrochlore oxides such as $Pr_2Ir_2O_7$ [16], the noncoplanarity of spins in these so-called spin-ice compounds is mainly created by a strong uniaxial anisotropy. The electron-driven magnetic instability in pyrochlore spin ice at quarter filling will be briefly discussed at the end of the Letter.

We begin with the isotropic Kondo-lattice Hamiltonian on the pyrochlore lattice:

$$H = -t\sum_{\langle ij\rangle}(c_{i\alpha}^{\dagger}c_{j\alpha} + \text{H.c.}) + J\sum_{\langle ij\rangle}\mathbf{S}_i \cdot \mathbf{S}_j$$
$$+ K\sum_i \mathbf{S}_i \cdot c_{i\alpha}^{\dagger}\boldsymbol{\sigma}_{\alpha\beta}c_{i\beta}. \quad (1)$$

The first term describes electron hopping between nearest-neighbor sites; t is the transfer integral and $c_{i\alpha}^{\dagger}$ creates an electron with spin α on site i. The second term represents the superexchange interaction between neighboring localized spins $\mathbf{S}_i$. The itinerant electrons interact with the localized spins through an on-site exchange coupling K as described by the third term, where $\boldsymbol{\sigma}_{\alpha\beta}$ is a vector of the Pauli matrices. Here we consider the classical limit $|\mathbf{S}_i| = S \gg 1$ of the localized spins. In this limit, the electron spectrum is independent of the sign of K, and the eigenstates corresponding to opposite signs are connected by a global gauge transformation [13].

We first consider the tight-binding spectrum of electrons on the pyrochlore lattice. In momentum space, the hopping Hamiltonian [first term in Eq. (1)] is expressed as

$H_t = \sum_{m,n}\sum_{\mathbf{k},\alpha}\tau_{mn}(\mathbf{k})c_{m\alpha}^{\dagger}(\mathbf{k})c_{n\alpha}(\mathbf{k})$, where m and n are sublattice indices and the hopping matrix is

$$\tau(\mathbf{k}) = -2t\begin{pmatrix} 0 & c_{yz} & c_{zx} & c_{xy} \\ c_{yz} & 0 & \bar{c}_{xy} & \bar{c}_{zx} \\ c_{zx} & \bar{c}_{xy} & 0 & \bar{c}_{yz} \\ c_{xy} & \bar{c}_{zx} & \bar{c}_{yz} & 0 \end{pmatrix}. \quad (2)$$

We have introduced $c_{ab} = \cos[(k_a + k_b)/4]$ and $\bar{c}_{ab} = \cos[(k_a - k_b)/4]$ and set the length of a cubic unit cell $a = 1$. This hopping matrix can be exactly diagonalized, giving rise to energy bands shown in Fig. 1(d). The spectrum consists of two degenerate flat bands $\varepsilon_{\mathbf{k}}^{\text{flat}} = 2t$ and two dispersive bands:

$$\varepsilon_{\mathbf{k}}^{\pm} = -2t(1 \mp \sqrt{1 + \mathcal{Q}_{\mathbf{k}}}), \quad (3)$$

where $\mathcal{Q}_{\mathbf{k}} = \cos\frac{k_x}{2}\cos\frac{k_y}{2} + \cos\frac{k_y}{2}\cos\frac{k_z}{2} + \cos\frac{k_z}{2}\cos\frac{k_x}{2}$. These two branches touch each other along the diagonal lines of the square faces of the Brillouin zone [Fig. 1(b)].

At quarter filling the lowest band $\varepsilon_{\mathbf{k}}^-$ is completely filled. The corresponding Fermi "surface" is determined by $\varepsilon_{\mathbf{k}}^+ = \varepsilon_{\mathbf{k}}^-$ and consists of diagonal lines $2\pi(x, 0, 1)$, and so on, on the square faces of the zone boundary. The Fermi energy lies exactly at $E_F = -2t$. Noting that $2\pi(x, 0, 1) \equiv 2\pi(1 - x, 1, 0)$ module a reciprocal lattice vector, these diagonal lines are topologically equivalent to three closed loops, or circles, intersecting with each other at the X points of the Brillouin zone [Figs. 1(b) and 1(c)]. In the vicinity of these Fermi lines, the spectrum has the singular form $\varepsilon_{\mathbf{k}}^{\pm} \approx E_F \pm C_{\varphi}|\mathbf{k}_{\perp}|$, where $\mathbf{k}_{\perp}$ is the perpendicular component of electron momentum.

Perfect nesting of the Fermi surface refers to the existence of wave vectors $\mathbf{Q}_i$ connecting large parallel areas of the surface such that $\varepsilon(\mathbf{k}) = \varepsilon(\mathbf{k} + \mathbf{Q}_i)$ for *all* wave vectors $\mathbf{k}$ on the Fermi surface. This condition, in general, cannot be satisfied for a generic Fermi surface in two or three dimensions. However, the Fermi surface in our case consists of three sets of parallel Fermi lines and can be perfectly nested by three wave vectors $\mathbf{Q}_1 = 2\pi(1, 0, 0)$, $\mathbf{Q}_2 = 2\pi(0, 1, 0)$, and $\mathbf{Q}_3 = 2\pi(0, 0, 1)$. For example, wave vectors on the two blue Fermi lines $\mathbf{k} = 2\pi(1, 0, z)$ and $\mathbf{k}' = 2\pi(0, 1, z)$, both belonging to the blue circle in Fig. 1(c), are connected by $\mathbf{Q}_3$ up to a reciprocal lattice vector. The van Hove singularity of the density of states at the Fermi level gives rise to a logarithmically divergent Lindhard susceptibility: $\chi(\mathbf{q}) \sim -\log|\mathbf{q} - \mathbf{Q}_{\eta}|$, indicating a nesting-induced weak-coupling instability.

To investigate possible magnetic ordering due to perfect nesting of the Fermi lines, we consider spin orders which can be expanded as

$$\mathbf{S}_i = \mathbf{S}_m(\mathbf{r}) = \sum_{\eta=0}^{3}\mathbf{M}_{m,\eta}e^{i\mathbf{Q}_{\eta}\cdot\mathbf{r}}, \quad (4)$$

where m is the sublattice index and $\mathbf{r}$ denotes the position of the Bravais (fcc) lattice point. In order to accommodate, e.g., ferromagnetic ordering, we have included a $\mathbf{Q}_0 = 0$

component in the above expansion. The unit cell of this
multiple-**Q** magnetic order is extended to the conventional
cubic unit cell which contains 16 spins.

Next we consider the on-site Hund's exchange which
couples electrons to the localized spins. In momentum
space, the multiple-**Q** magnetic order introduces couplings
between a pair of electrons whose momenta differ by the
nesting vectors $\mathbf{Q}_\eta$:

$$H_K = \sum_{\xi,\eta} \sum_{\alpha,\beta} \sum_{m,\mathbf{k}}' c_{m\alpha}^\dagger(\mathbf{k} + \mathbf{Q}_\xi) \mathcal{M}_{\xi\alpha,\eta\beta}^{(m)} c_{m\beta}(\mathbf{k} + \mathbf{Q}_\eta). \quad (5)$$

Here the prime indicates that the momentum summation is
restricted to the reduced Brillouin zone [see Fig. 3(b)], and
the coupling coefficients are given by

$$\mathcal{M}_{\xi\alpha,\eta\beta}^{(m)} = K\Delta_{\xi\eta,\zeta}(\mathbf{M}_{m,\zeta} \cdot \boldsymbol{\sigma}_{\alpha\beta}) e^{i(\mathbf{Q}_\xi - \mathbf{Q}_\eta) \cdot \mathbf{d}_m}, \quad (6)$$

where $\mathbf{d}_m$ denotes basis vectors of the pyrochlore lattice.
Momentum conservation of the coupling is encoded in
the symbol $\Delta_{\xi\eta,\zeta}$, which is symmetric with respect to
the first two indices. The nonzero components include
$\Delta_{01,1} = \Delta_{02,2} = \Delta_{03,3} = \Delta_{23,1} = \Delta_{31,2} = \Delta_{12,3} = 1$.

For a given set of Fourier components $\mathbf{M}_{m,\eta}$, diagonal-
ization of the electron Hamiltonian $H_t + H_K$ gives a total of
32 energy bands. At quarter filling, the ground-state energy
of electrons E_e is obtained by filling the lowest eight bands.
However, the determination of the minimum-energy state is
not straightforward because of the large number of variables
required to describe the complex magnetic order; one needs
32 variables to specify the 16 classical spins in a quadrupled
unit cell. To this end, we employ the simulated annealing
method to minimize the energy functional $E_e(\mathbf{M}_{m,\eta})$. For
$J = 0$ and $K < K_c \approx 4.32t$, numerical minimization yields
a noncoplanar magnetic order shown in Fig. 2 starting from
different initial configurations. Above the critical coupling
$K > K_c$, the ferromagnetic order with $\mathbf{S}_i = S\hat{\mathbf{n}}$ takes over
and becomes the ground state.

To characterize the noncoplanar spin structure, we
introduce three order parameters $\mathbf{L}_1 = (\mathbf{S}_0 + \mathbf{S}_1 - \mathbf{S}_2 - \mathbf{S}_3)/4S$, and so on [4], which measure the staggered
magnetizations of a tetrahedron; the spin subscript indi-
cates the corresponding sublattice. A unit cell of the mag-
netic order is shown in Fig. 2(a), where the magnetic states
of type-I tetrahedra are described by order parameters

$$\mathbf{L}_1 = \frac{\hat{\mathbf{n}}_1}{\sqrt{3}} e^{i\mathbf{Q}_3 \cdot \mathbf{r}}, \quad \mathbf{L}_2 = \frac{\hat{\mathbf{n}}_2}{\sqrt{3}} e^{i\mathbf{Q}_1 \cdot \mathbf{r}}, \quad \mathbf{L}_3 = \frac{\hat{\mathbf{n}}_3}{\sqrt{3}} e^{i\mathbf{Q}_2 \cdot \mathbf{r}}. \quad (7)$$

Here $\hat{\mathbf{n}}_r$'s are three mutually orthogonal unit vectors.
Remarkably, the noncoplanar magnetic order is a simulta-
neous ground state of the intersite exchange interaction. To
see this, we note that the superexchange term in Eq. (1) can
be recast to $H_J = (J/2)\sum_\boxtimes |\mathbf{M}_\boxtimes|^2$, where $\mathbf{M}_\boxtimes = \sum_{m=0}^3 \mathbf{S}_m$
is the total magnetization of a tetrahedron. For the mag-
netic order shown in Fig. 2, the total spin of every tetrahe-
dron, including both types, vanishes identically, hence
minimizing the exchange energy. This result also indicates
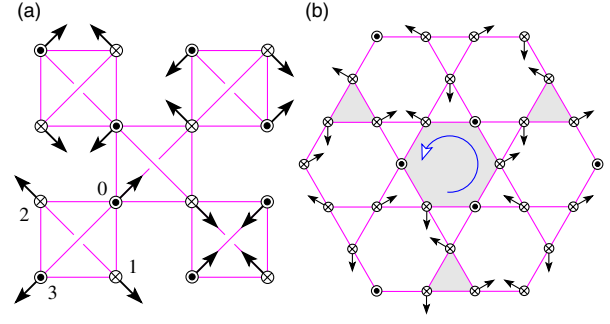

FIG. 2 (color online). (a) A unit cell of the noncoplanar
magnetic order viewed from the c axis. Here we choose $\hat{\mathbf{n}}_1 = \hat{\mathbf{a}}$, $\hat{\mathbf{n}}_2 = \hat{\mathbf{b}}$, and $\hat{\mathbf{n}}_3 = \hat{\mathbf{c}}$ in Eq. (7). (b) Chiral structure of the same
magnetic order projected onto a (111) kagome plane. The $\odot$ and
$\otimes$ symbols denote a spin component coming out of and into the
plane, respectively. The same handedness (right-handed in this
case) is observed in other kagome planes.

that the ferromagnetic order favored by a large Hund's
coupling K is suppressed by the antiferromagnetic intersite
exchange.

Figure 3(a) shows the electron band structure corre-
sponding to the noncoplanar magnetic order. The spectrum
is at least doubly degenerate thanks to a combined lattice
translation and spin rotation symmetry. Because of the
nesting effect, a charge gap opens between the lower four
pairs of bands and other high energy branches. It is known
that the electron experiences a fictitious magnetic field
proportional to the spin chirality $\chi_{ijk} = \mathbf{S}_i \cdot \mathbf{S}_j \times \mathbf{S}_k$
when hopping around a triangular loop [16]. Although
χ_{ijk} is nonzero in the noncoplanar structure, the contribu-
tions from the four triangular faces of a tetrahedron cancel
each other due to a monopolelike spin configuration. The
noncoplanar magnetic order thus does not exhibit a sponta-
neous quantum Hall effect.

The magnetic structure itself, nonetheless, breaks the
chiral symmetry. This is best illustrated by projection of
the triple-**Q** magnetic order onto a (111) kagome plane
which shows hexagons and triangles with a definite hand-
edness [Fig. 2(b)]. More specifically, we introduce a scalar
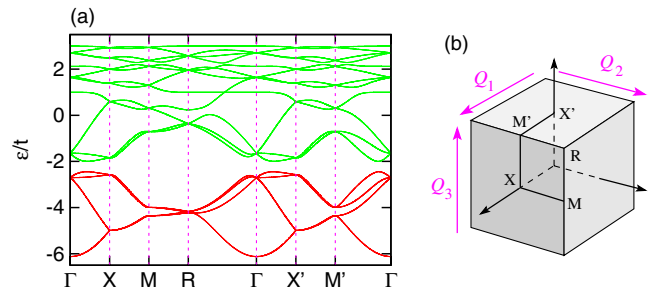chirality for a tetrahedron in the antiferromagnetic state:

FIG. 3 (color online). (a) Electron band structure corresponding
to the noncoplanar magnetic order shown in Fig. 2. The Hund's
coupling is $K = t$ and superexchange constant $J = 0$. (b) The
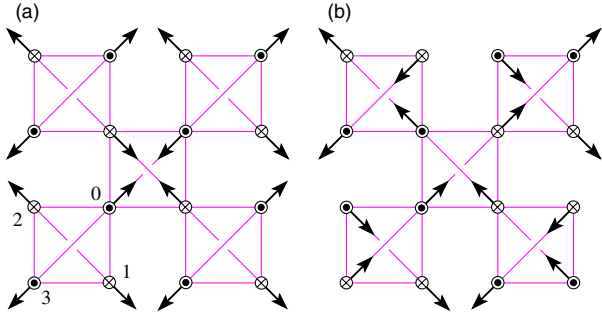reduced Brillouin zone with high-symmetry points and lines.

FIG. 4 (color online).   (a) All-in all-out structure. (b) The 2-in–2-out magnetic order with wave vector $\mathbf{Q}_3 = 2\pi(0, 0, 1)$. The $\odot$ and $\otimes$ symbols again denote a spin component coming out of and into the plane, respectively.

$$\chi_{\boxtimes} = 3\sqrt{3}\mathbf{L}_1 \cdot \mathbf{L}_2 \times \mathbf{L}_3. \tag{8}$$

The noncoplanar magnetic order shown in Fig. 2 has the maximum chirality $\langle \chi_{\boxtimes} \rangle = +1$, where the average is over both types of tetrahedra. This is to be contrasted with the so-called all-in all-out structure [Fig. 4(a)] in which the two types of tetrahedra have opposite chiralities $\langle \chi_{\mathrm{I}} \rangle = -\langle \chi_{\mathrm{II}} \rangle$; the average chirality is thus zero.

The model described by Eq. (1) with a negative K was recently investigated in Ref. [11] with the aid of Monte Carlo simulations. The authors also considered the special case of quarter filling. However, since the simulations were performed assuming a large Hund's coupling, the noncoplanar magnetic order shown in Fig. 2 was not observed in their simulations. Although the fine structure of the electron Fermi surface is absent in small finite systems, the noncoplanar magnetic order could be obtained in Monte Carlo simulations at small Hund's coupling by using techniques such as twisted boundary conditions [11].

We now turn to the spin-ice compounds where the rotational symmetry is explicitly broken by a strong easy-axis anisotropy $H_D = -D\sum_i (\mathbf{S}_i \cdot \hat{\mathbf{e}}_m)^2$. The effective degrees of freedom become discrete Ising variables as spins are forced to point along the local $\langle 111 \rangle$ directions, i.e., $\mathbf{S}_i = \pm S\hat{\mathbf{e}}_m$. At filling factor $\nu = 1/4$, we found a ground state with the all-in all-out magnetic structure [Fig. 4(a)] in the $J = 0$ limit. It remains the ground state in the presence of antiferromagnetic exchange as $\mathbf{M}_{\boxtimes} = 0$ on all tetrahedra. In spin-ice compounds, however, the nearest-neighbor exchange has a ferromagnetic sign, i.e., $J = -|J|$. Assuming $D \gg |J| \gg t, K$, numerical minimization yields a single-$\mathbf{Q}$ magnetic order consisting of 2-in–2-out tetrahedra [Fig. 4(b)]: the magnetizations of type-I and type-II tetrahedra point along the a and b axes, respectively, with their sign alternating between adjacent ab planes.

Both magnetic orders shown in Fig. 4 were observed in a recent Monte Carlo study on a metallic pyrochlore spin ice [10]. Instead of tackling the Kondo-lattice model directly, the simulations in Ref. [10] were performed assuming a long-range RKKY interaction between localized spins. The case of quarter filling with a 2-in–2-out magnetic ground state lies very close to the boundary separating these two spin

structures [10]. Since the RKKY interaction is derived by integrating out the electrons with a spherical Fermi surface, this approach is valid only at small filling fractions where the spectrum can be approximated by a quadratic dispersion.

In summary, we have studied a model of itinerant electrons interacting with localized classical spins on the pyrochlore lattice. At quarter filling, we showed that a noncoplanar magnetic order emerges as the ground state of the rotationally invariant Hamiltonian. The magnetic structure characterized by a nonzero order parameter $\chi_{\boxtimes}$ also breaks the chiral symmetry. Since from the symmetry viewpoint the chiral transition need not coincide with the magnetic ordering, a chiral phase with $\langle \chi_{\boxtimes} \rangle \neq 0$ but no spin order $\langle \mathbf{L}_i \rangle = 0$ could occur at finite temperatures. Such a scenario was recently reported in spin-ice compound $Pr_2Ir_2O_7$, where a nonzero spin chirality was observed in an intermediate phase with disordered spins [17]. Future studies, especially large-scale Monte Carlo simulations, could numerically demonstrate the noncoplanar magnetic structure and explore the possibility of the partially ordered chiral phase.

[1] R. Moessner and J. T. Chalker, Phys. Rev. Lett. **80**, 2929 (1998); Phys. Rev. B **58**, 12 049 (1998).
[2] S.-H. Lee *et al.*, Phys. Rev. Lett. **84**, 3718 (2000); J.-H. Chung *et al.*, Phys. Rev. Lett. **95**, 247204 (2005).
[3] O. Tchernyshyov, R. Moessner, and S. L. Sondhi, Phys. Rev. Lett. **88**, 067203 (2002); Phys. Rev. B **66**, 064403 (2002).
[4] G.-W. Chern, C. Fennie, and O. Tchernyshyov, Phys. Rev. B **74**, 060405(R) (2006).
[5] S.-H. Lee *et al.*, Phys. Rev. Lett. **93**, 156407 (2004).
[6] V. O. Garlea *et al.*, Phys. Rev. Lett. **100**, 066404 (2008).
[7] O. Tchernyshyov, Phys. Rev. Lett. **93**, 157206 (2004).
[8] G.-W. Chern and N. Perkins, Phys. Rev. B **80**, 180409(R) (2009); G.-W. Chern, N. Perkins, and Z. Hao, Phys. Rev. B **81**, 125127 (2010).
[9] D. Ikoma, H. Tsuchiura, and J. Inoue, Phys. Rev. B **68**, 014420 (2003).
[10] A. Ikeda and H. Kawamura, J. Phys. Soc. Jpn. **77**, 073707 (2008).
[11] Y. Motome and N. Furukawa, Phys. Rev. Lett. **104**, 106407 (2010); J. Phys. Conf. Ser. **200**, 012131 (2010).
[12] C. Lacroix, J. Phys. Soc. Jpn. **79**, 011008 (2010).
[13] I. Martin and C. D. Batista, Phys. Rev. Lett. **101**, 156402 (2008).
[14] Y. Akagi and Y. Motome, J. Phys. Soc. Jpn. **79**, 083711 (2010).
[15] Y. Kato, I. Martin, and C. D. Batista, arXiv:1009.3059.
[16] S. Nakatsuji *et al.*, Phys. Rev. Lett. **96**, 087204 (2006).
[17] Y. Machida *et al.* Nature (London) **463**, 210 (2010).